

# MARE: Multimodal Alignment and Reinforcement for Explainable Deepfake Detection via Vision-Language Models

Wenbo xu<sup>1</sup> Wei Lu<sup>1</sup> Xiangyang Luo<sup>2</sup> Jiantao Zhou<sup>3</sup>

## Abstract

Deepfake detection is a widely researched topic that is crucial for combating the spread of malicious content, with existing methods mainly modeling the problem as classification or spatial localization. The rapid advancements in generative models impose new demands on Deepfake detection. In this paper, we propose multimodal alignment and reinforcement for explainable Deepfake detection via vision-language models, termed MARE, which aims to enhance the accuracy and reliability of Vision-Language Models (VLMs) in Deepfake detection and reasoning. Specifically, MARE designs comprehensive reward functions, incorporating reinforcement learning from human feedback (RLHF), to incentivize the generation of text-spatially aligned reasoning content that adheres to human preferences. Besides, MARE introduces a forgery disentanglement module to capture intrinsic forgery traces from high-level facial semantics, thereby improving its authenticity detection capability. We conduct thorough evaluations on the reasoning content generated by MARE. Both quantitative and qualitative experimental results demonstrate that MARE achieves state-of-the-art performance in terms of accuracy and reliability.

## 1. Introduction

Concerns about the security of AI have accompanied its evolution from the beginning. A recent study shows that more than half of new articles on the internet are AI-generated (Jose et al., 2025), surpassing human-created content. The

<sup>1</sup>School of Computer Science and Engineering, MoE Key Laboratory of Information Technology, Guangdong Province Key Laboratory of Information Security Technology, Sun Yat-sen University, Guangzhou 510006, China <sup>2</sup>State Key Laboratory of Mathematical Engineering and Advanced Computing, Zhengzhou 450002, China. <sup>3</sup>Department of Computer and Information Science, University of Macau.. Correspondence to: Wei Lu <luwei3@mail.sysu.edu.cn>.

Preprint. January 29, 2026.

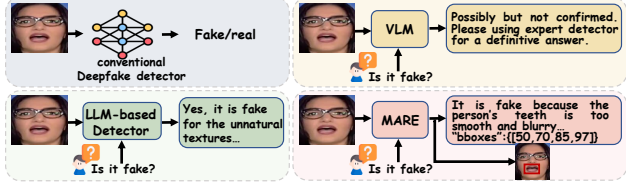


Figure 1. Illustration of different Deepfake detection methods. The conventional Deepfake detectors provide a discriminative decision. The existing LLM-based methods generate plain textual reasoning content. While the pre-trained VLMs struggle to satisfy Deepfake reasoning demands. Our method generates detailed forgery traces analysis and provides spatial localization information for supporting evidence.

proliferation of AI-generated content has varying degrees of impact on individuals, society, and nations. To mitigate the misuse of generative AI on face data, Deepfake detection has emerged as a popular research topic in recent years. Its primary purpose is to identify forged face images or videos, involving tasks such as binary authenticity detection (Yin et al., 2024), spatial forgery localization (Huang et al., 2025), and temporal forgery localization (Xu et al., 2025b).

Existing Deepfake detection methods primarily exploit specific forgery traces within forged face data, such as blurred edges (Shiohara & Yamasaki, 2022), spatial inconsistencies (Zhang et al., 2025a), and temporal jitter (Xu et al., 2025a), to obtain a discriminative detection result. With the rapid advancement of generative models, particularly Large Language Models (LLMs) and Vision-Language Models (VLMs), new identification demands have emerged for Deepfake detection and reasoning. Several recent methods have attempted to leverage LLMs for explainable Deepfake detection. For example, M2F2-Det (Guo et al., 2025) enhances the explainability of Vicuna-7B (Chiang et al., 2023) by integrating the forgery prompt learning and the CLIP's multimodal representation ability. KFD (Yu et al., 2025) proposes aligning face images with textual descriptions to generate forgery consistency maps, which achieves multimodal alignment through prompt learning. RAIDX (Li et al., 2025a) integrates retrieval-augmented generation and group relative policy optimization to enhance the detection accuracy and decision explainability of LLMs. The aforementioned methods primarily rely on combining prompt

engineering with LLMs, which enhance the ability of explainable Deepfake detection through elaborate prompt design. In this paper, we focus on directly leveraging VLMs for Deepfake detection. By integrating reinforcement learning and multimodal alignment of reasoning content, we aim to enhance the accuracy and reliability of VLMs in Deepfake detection and reasoning. VLMs exhibit superior performance in associating textual and visual modalities, thus generating more reliable content by maintaining multimodal representation alignment during the reasoning process (Zhai et al., 2024). While existing pre-trained VLMs perform well in scenarios involving strong semantic signals, such as Visual Question Answering and Image Captioning, they tend to underperform in the task of Deepfake detection scenario. The primary reason is that forged face images are often visually difficult to distinguish from genuine ones, since the forgery traces are typically subtle or imperceptible. Therefore, it is necessary to enhance existing pre-trained VLMs for the specific scenario of Deepfake detection.

Reinforcement learning (RL) has been demonstrated to enhance the reasoning capability of VLMs through feedback on their outputs (Shen et al., 2025). Compared to Supervised Fine-Tuning (SFT), the RL-based optimization strategy could mitigate model hallucinations and encourage the model to explore solutions that reflect human preferences. By leveraging the reward mechanism in RL, we could not only incentivize the VLMs to capture subtle visual traces in forged face images, but also facilitate multimodal alignment in the reasoning process (Li et al., 2025b). This significantly motivates the VLMs to explore and generate more accurate and reliable Deepfake detection and reasoning content.

In this paper, we propose MARE: multimodal alignment and reinforcement for explainable Deepfake detection via vision-language models. The primary objective of MARE is to enhance the accuracy and reliability of VLMs in Deepfake detection and reasoning. Under the reinforcement learning from human feedback (RLHF) paradigm, we first design a comprehensive reward mechanism. Specifically, MARE designs multi-dimensional reward functions to incentivize the reasoning capability of VLMs in Deepfake detection, which include format, accuracy, text relevance, ROI, and alignment rewards (see Section 3.3 for details). To fulfill the data requirements for fine-tuning, a Deepfake multimodal alignment dataset is introduced by augmenting the existing image-text Deepfake dataset with aligned spatial localization information. MARE also introduces a forgery disentanglement module to capture intrinsic forgery traces for precise authenticity identification, which explicitly disentangles the face image into identity, structural, and forgery traces features based on representation learning. The main contributions are summarized as follows:

- MARE employs a multimodal alignment strategy to en-

hance the reasoning capability of VLMs for Deepfake detection and reasoning, which incentivizes the VLMs to explore and generate more accurate and reliable reasoning content under RLHF paradigm.

- MARE introduces a novel forgery disentanglement module to capture intrinsic forgery traces within face images, which improves the authenticity detection capability through representation learning.
- MARE achieves state-of-the-art performance in Deepfake detection and reasoning, which has been validated by extensive quantitative and qualitative evaluations on multiple datasets.

## 2. Related Works

**Deepfake detection.** Deepfake detection primarily focuses on binary classification, which aims to discriminate the authenticity of a given image or video. Various effective strategies have been proposed, including data augmentation (Yin et al., 2024), biometric information analysis (Xu et al., 2023), and attention mechanisms (Zhao et al., 2021). Besides, some methods have also investigated the spatial localization task and temporal localization task to cope with different detection scenarios (Zhang et al., 2025a; Xu et al., 2025a). These methods basically provide a discriminative decision for a given face data, lacking additional forensic information for humans. Recently, researchers have explored utilizing LLMs to generate the textual reasoning content about forgery traces, which enables the Deepfake detection to be more explainable (Guo et al., 2025; Yu et al., 2025). The LLM-based methods typically fine-tune models using image-text pairs, where the answers usually consist of only text information about forgery traces. It should be noted that a conventional Deepfake detector is often employed as an expert network to guide the LLM’s reasoning process. In this paper, MARE introduces additional spatial information to motivate the VLM to generate more reliable reasoning content with text-spatial alignment.

**Multimodal alignment in VLMs.** Alignment is crucial for improving the downstream task accuracy, safety, and reliability of VLMs (Li et al., 2025b). The general alignment algorithm is reinforcement learning from human feedback (RLHF). RLHF is a machine learning technique that uses human feedback to train and align models for performing reasoning tasks more aligned with human preferences (Li et al., 2024; Xie et al., 2025). The core principle of RLHF is to construct human feedback annotation data and design reward mechanisms. MM-RLHF (Zhang et al., 2025b) constructs a high-quality, fine-grained dataset with 120k preference comparison pairs to advance the alignment of VLMs. Group relative policy optimization utilizes rule-based reward to improve the models’ chain-of-thought ability for

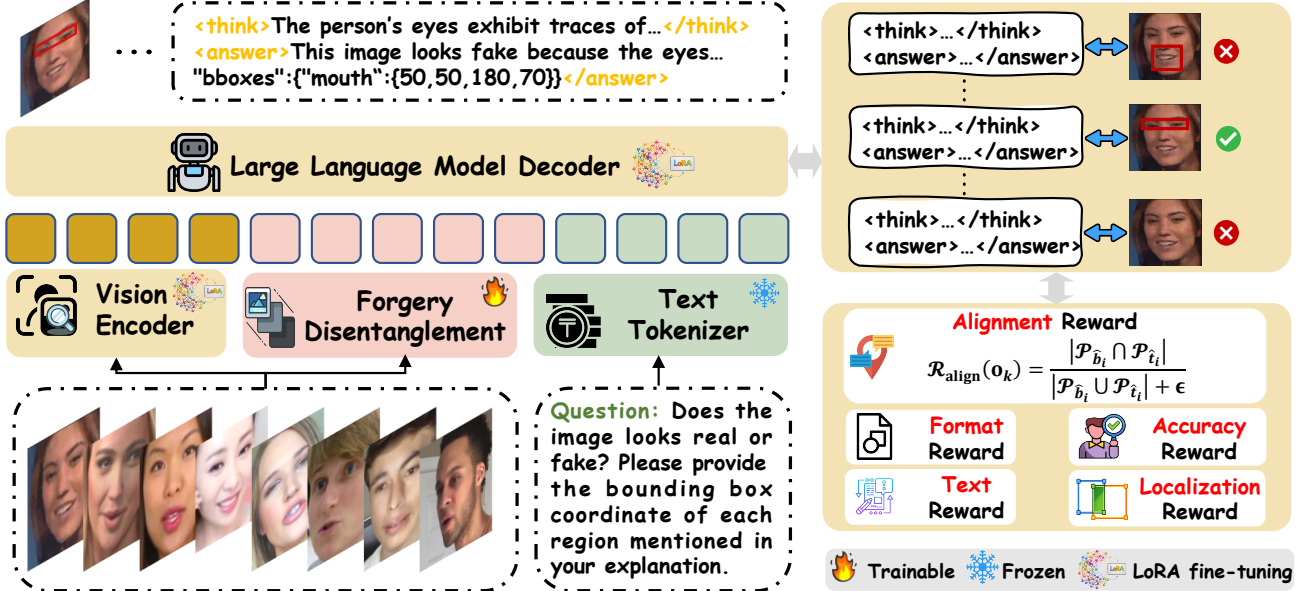


Figure 2. Diagrammatic overview of the proposed MARE framework. The reward functions and RLHF algorithm are displayed on the right side (see Section 3.3 for details). The vision encoder, text tokenizer, and large language model decoder are key components of VLM. The forgery disentanglement module is introduced for forgery traces extraction (see Section 3.4 for details). During the inference phase, MARE generates text-spatially aligned reasoning content for a given image-text query.

more accurate and reliable reasoning content (Shao et al., 2024). RLHF has become one of the most popular and effective paradigms to align VLMs. However, existing LLM-based Deepfake detectors have insufficient exploration of alignment (Meng et al., 2025). In this paper, MARE initially constructs a preference text-spatially aligned dataset. Based on these data, MARE introduces elaborate reward functions to improve the accuracy and reliability of VLMs in Deepfake decision attribution.

### 3. Method

In this section, the specific framework and training details of the proposed MARE are elaborated. For clarity, an overview of MARE is first introduced.

#### 3.1. Overview

To enhance the accuracy and reliability of VLMs in Deepfake detection and reasoning, we propose MARE under the RLHF paradigm. The diagrammatic overview is shown in Figure 2. We design comprehensive reward functions and construct a human-preference dataset to incentivize the VLMs to generate text-spatially aligned reasoning content. Meanwhile, MARE introduces a forgery disentanglement module (FDM) to capture intrinsic forgery traces for precise authenticity detection.

Specifically, we construct a Deepfake multimodal alignment dataset  $\mathcal{D}_{ma} = \{\langle v_i, q_i, t_i, b_i \rangle\}_{i=1}^N$ , where  $v_i, q_i, t_i$ ,

$b_i$  denote the face image, question, textual description, and spatial bounding boxes, respectively. During the RLHF fine-tuning process, given an input pair  $\langle v_i, q_i \rangle$ , a set of candidate reasoning responses  $\mathcal{O} = \{o_k = (\hat{t}_k, \hat{b}_k)\}_{k=1}^K$  will be generated by the VLM. Leveraging the comprehensive reward functions and the ground truth  $\langle t_i, b_i \rangle$ , MARE calculates rewards to estimate the relative advantage of each response. This process drives gradient updates to optimize the policy of VLM, refining its chain-of-thought capability for Deepfake detection and reasoning. Besides, MARE introduces FDM to capture intrinsic forgery traces caused by the face forgery process. This module disentangles the face image into identity, structural, and forgery traces features based on representation learning.

In the inference phase, MARE generates text-spatially aligned reasoning content  $\langle \hat{t}_i, \hat{b}_i \rangle$  for a given query  $\langle v_i, q_i \rangle$ , where  $\hat{t}_i$  is the textual reasoning content that contains the authenticity detection result and related explanation,  $\hat{b}_i$  provides the spatial localization of regions mentioned in  $\hat{t}_i$ .  $\hat{t}_i$  and  $\hat{b}_i$  provide mutual validation to improve the accuracy and reliability of reasoning content.

#### 3.2. Multimodal Alignment

Alignment could improve the accuracy, safety, and reliability of VLMs in the downstream task (Li et al., 2025b). In the Deepfake forensic domain, it is particularly crucial to enhance the accuracy and reliability of reasoning content through multimodal alignment. In this paper, the objective

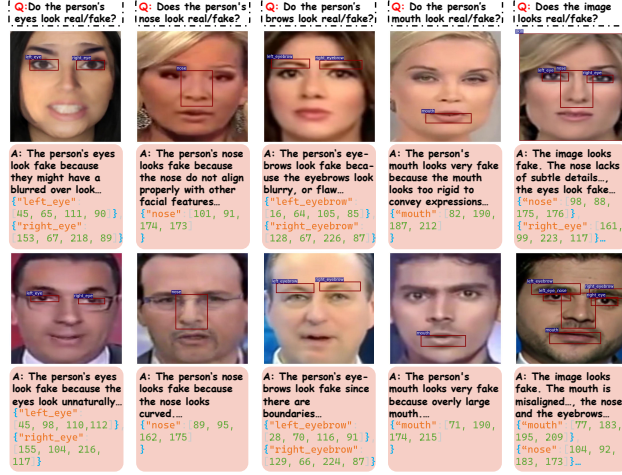


Figure 3. Examples of the Deepfake multimodal alignment dataset (DMA).

of multimodal alignment is to incentivize the VLM to generate reasoning content that aligns textual and spatial information. For instance, if the text describes forgery traces in the eyes, the reasoning output should provide the corresponding bounding boxes for the eyes region. This mechanism could not only mitigate the VLM’s hallucinations but also enhance the reliability of the reasoning content.

We construct the Deepfake multimodal alignment dataset (DMA) by augmenting the existing image-text dataset (Zhang et al., 2024; Yu et al., 2025), denoted as  $\mathcal{D}_{src} = \{\langle v_i, q_i, t_i \rangle\}_{i=1}^N$ , where  $v_i$  indicates the face image,  $q_i$  is a query question, and  $t_i$  is the ground-truth textual description about authenticity and detailed analysis. We propose a two-stage extraction and localization pipeline. Specifically, a set of facial regions  $\mathcal{P}_{key}$  is defined (e.g., eyes, nose, or mouth, see appendix B for details). We perform keyword retrieval  $\mathbb{E}(\cdot, \cdot)$  for each  $t_i$  to extract the specific regions  $r_i$ . Then, a face landmark detection model  $\mathbb{L}(\cdot, \cdot)$  is utilized to locate the spatial bounding boxes  $b_i$  from the face image  $v_i$ . The pipeline is formulated as:

$$r_i = \mathbb{E}(t_i, \mathcal{P}_{key}) \quad b_i = \mathbb{L}(v_i, r_i) \quad (1)$$

Finally, the DMA dataset  $\mathcal{D}_{ma} = \{\langle v_i, q_i, t_i, b_i \rangle\}_{i=1}^N$  is obtained, which serves as the foundation for the subsequent multimodal alignment fine-tuning. The examples of DMA are shown in Figure 3.

### 3.3. Reinforcement Learning Reward Design

We fine-tune VLMs with the reinforcement learning algorithm (e.g., GRPO (Shao et al., 2024)). To incentivize the reasoning capability of VLMs in Deepfake detection and reasoning, we design a set of task-specific reward functions, including format reward  $\mathcal{R}_f$ , accuracy reward  $\mathcal{R}_a$ , text relevance reward  $\mathcal{R}_t$ , ROI reward  $\mathcal{R}_r$ , and alignment reward

$\mathcal{R}_{align}$ .

**Format reward.** Format reward is to check whether the VLM’s responses follow the human preferences format. Specifically, MARE requires the model to present the reasoning paths enclosed within  $\langle \text{think} \rangle \dots \langle / \text{think} \rangle$  tags. The final reasoning result within  $\langle \text{answer} \rangle \dots \langle / \text{answer} \rangle$  tags should contain two parts: a "explanation" field with a string value describing why the face image is real or fake, and a "bboxes" field listing the bounding box of each region mentioned in the "explanation" that serves as evidence. Formally,

$$\mathcal{R}_f(o_k) = \begin{cases} 1.0, & \text{if } o_k \text{ fulfills the format} \\ 0, & \text{otherwise} \end{cases} \quad (2)$$

where  $o_k$  denotes the  $k$ -th candidate response for a given fine-tuning instruction  $\mathcal{D}_{ma}^{(i)}$ .

**Accuracy reward.** To support the Deepfake detection and reasoning task, MARE introduces an accuracy reward  $\mathcal{R}_a$  based on the correctness of authenticity prediction within the response. Specifically, we extract keyword "fake" or "real" from the "explanation" field. Serving as a basic and essential signal,  $\mathcal{R}_a$  is to incentivize VLMs explore a valid chain-of-thought path for precise Deepfake detection. Formally,

$$\mathcal{R}_a(o_k) = \begin{cases} 1.0, & \text{if } d_k = g^{(i)} \\ 0, & \text{otherwise} \end{cases} \quad (3)$$

where  $d_k$  denotes the prediction result of authenticity in  $o_k$ , and  $g^{(i)}$  is the corresponding ground truth label in  $\mathcal{D}_{ma}^{(i)}$ .

**Text relevance reward.** Text relevance reward  $\mathcal{R}_t$  is designed to incentivize the VLM to generate responses similar to the annotated textual description. Specifically, we utilize a sentence encoder (e.g., SentenceTransformer (Wang et al., 2020)) to map  $t_i$  and  $\hat{t}_i^{(k)}$  into embeddings, where  $t_i$  is the human annotated textual description in  $\mathcal{D}_{ma}^{(i)}$ , and  $\hat{t}_i^{(k)}$  is the generated textual content in the  $k$ -th candidate response  $o_k$ .  $\mathcal{R}_t$  is then obtained by calculating the similarity between these embeddings. Formally,

$$\mathcal{R}_t(o_k) = \max \left( 0, \cos \left( \Phi(\hat{t}_i^{(k)}), \Phi(t_i) \right) \right) \quad (4)$$

where  $\Phi(\cdot)$  indicates the sentence encoder,  $\cos(\cdot, \cdot)$  computes the cosine similarity between the two embedding vectors.

**Region of interest reward.** To enhance the VLM’s capability in localizing facial regions, MARE introduces a region of interest (ROI) reward  $\mathcal{R}_r$ . Specifically, the response  $o_k$  is required to contain a "bboxes" field  $\hat{b}^{(k)}$ , which consists of pairs of facial regions and their corresponding

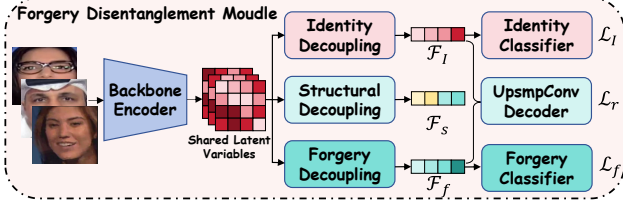


Figure 4. Illustration of the proposed forgery disentanglement detector (FDM). The diagrammatic structure of FDM is shown in the left panel, while the right panel depicts the structure of the adversarial classifier.

coordinates. The  $\mathcal{R}_r$  evaluates the localization performance to incentivize the VLM to identify the bounding boxes of facial regions. Formally,

$$\mathcal{R}_r(o_k) = \frac{1}{|\mathcal{P}|} \sum_{p \in \mathcal{P}} \text{IoU}(\hat{b}_{i,p}^{(k)}, b_{i,p}) \quad (5)$$

where  $b_i$  is the spatial bounding boxes in  $\mathcal{D}_{ma}^{(i)}$ ,  $\mathcal{P}$  denotes the set of facial regions (e.g., eyes, nose) present in both  $\hat{b}_i^{(k)}$  and  $b_i$ ,  $\hat{b}_{i,p}^{(k)}$  and  $b_{i,p}$  denote the predicted and ground truth bounding boxes for the specific part  $p$ , respectively.

**Alignment reward.** The alignment reward  $\mathcal{R}_{align}$  is designed to incentivize the VLM to generate text-spatially aligned reasoning content. This mechanism helps to mitigate the VLM's hallucinations. Then MARE could generate more reliable Deepfake detection and reasoning results. Specifically, for a candidate response  $o_k$ , we extract the set of facial regions  $\mathcal{P}_{\hat{b}_i}$  from "bbox" field, and the set of mentioned facial regions  $\mathcal{P}_{\hat{t}_i}$  from the "explanation" field. The higher the overlap between these two sets, the greater the alignment between textual and spatial reasoning content. Formally,

$$\mathcal{R}_{align}(o_k) = \frac{|\mathcal{P}_{\hat{b}_i} \cap \mathcal{P}_{\hat{t}_i}|}{|\mathcal{P}_{\hat{b}_i} \cup \mathcal{P}_{\hat{t}_i}| + \epsilon} \quad (6)$$

where  $|\cdot|$  denotes the cardinality of the set,  $\epsilon$  is a constant to prevent division by zero.

### 3.4. Forgery Disentanglement Module

Forgery traces in Deepfake face images usually emerge as subtle signals, such as blending boundaries, frequency anomalies, or inconsistent resolution. Therefore, it is necessary to make the model concentrate on subtle forgery traces rather than strong signals such as identity representation or high-level semantics. The forgery disentanglement module (FDM) decouples features from the given face image based on representation learning. The diagrammatic structure of FDM is illustrated in Figure 4.

Specifically, FDM first utilizes a backbone to obtain the shared latent representations  $\mathcal{F}$  of the given face image.  $\mathcal{F}$

are disentangled into identity features  $\mathcal{F}_I$ , structural features  $\mathcal{F}_s$ , and forgery trace features  $\mathcal{F}_f$ . To facilitate feature disentanglement, the FDM incorporates dedicated classifiers and loss functions to guide FDM training. The identity classifier utilizes  $\mathcal{F}_I$  to generate identity predictions, then calculates the identity prediction loss  $\mathcal{L}_I$  based on the ground truth identity annotations. Focal loss is utilized to guide the model to focus on challenging samples. Formally,

$$\mathcal{L}_I = -\frac{1}{N} \sum_{i=1}^N \sum_{j=1}^M \left[ y_{ij} \alpha_j (1 - \hat{y}_{ij})^\gamma \log(\hat{y}_{ij}) \right] \quad (7)$$

where  $N$  indicates the number of samples,  $M$  is the number of identities, and  $y_{ij} \in \{0, 1\}$  is the ground truth identity annotation.  $\hat{y}_{ij}$  denotes the predicted probability that sample  $\mathcal{D}_{ma}^{(i)}$  belongs to the  $j$ -th identity.  $\alpha_j$  is the balancing parameter for the  $j$ -th identity, and  $\gamma$  is the focusing parameter.

The primary objective of FDM is to capture intrinsic forgery traces from the detected face image. To provide explicit supervision for this disentanglement, FDM introduces a forgery classifier to perform binary authenticity discrimination based on  $\mathcal{F}_f$ . Then, the forgery prediction loss  $\mathcal{L}_f$  is obtained. Formally,

$$\mathcal{L}_f = -\frac{1}{N} \sum_{i=1}^N \left[ g_i \cdot \alpha (1 - \hat{g}_i)^\hat{\gamma} \log(\hat{g}_i) + (1 - g_i) \cdot (1 - \alpha) \hat{g}_i^\hat{\gamma} \log(1 - \hat{g}_i) \right] \quad (8)$$

where  $g_i \in \{0, 1\}$  is the ground truth of authenticity,  $\hat{g}_i$  denotes the authenticity prediction probability,  $\alpha$  and  $\hat{\gamma}$  are weighting factors.

Besides identity information and forgery traces, the face image also contains structural information, such as illumination, expressions, and head posture information. To prevent these factors from interfering with forgery detection, they are disentangled into structural features  $\mathcal{F}_s$ .  $\mathcal{F}_s$ ,  $\mathcal{F}_I$ , and  $\mathcal{F}_f$  are concatenated for initial feature reconstruction. This imposes an information constraint that maintains the stability of the disentanglement framework. Formally,

$$\mathcal{L}_r = \frac{1}{N} \sum_{i=1}^N \left( \mathcal{F}_i - \mathcal{F}_i^{(r)} \right)^2 \quad (9)$$

where  $\mathcal{F}_i$  is the shared latent representations, and  $\mathcal{F}_i^{(r)}$  is the reconstruction features.

### 3.5. Training and Inference

**Training.** MARE contains two training stages: supervised training for the FDM and reinforcement learning-based optimization for the VLM. First, the FDM is trained based

Table 1. The experimental results of intra-dataset detection. The best results are presented in red. The second-best values are in blue.

Methods	Venue	FF++		Celeb-DF		WDF		DFDC	
		Metric: Acc (%) ↑ / AUC (%) ↑							
MultiAtt (Zhao et al., 2021)	CVPR21	97.60	99.29	97.92	99.94	82.86	90.71	–	–
RECCE (Cao et al., 2022)	CVPR22	97.06	99.32	98.59	99.94	83.25	92.02	81.20	91.33
TALL (Xu et al., 2023)	ICCV23	98.65	99.87	97.57	98.55	–	–	–	76.78
TGN (She et al., 2024)	TIFS24	–	99.32	–	99.59	–	–	–	96.24
M2F2 (Guo et al., 2025)	CVPR25	98.79	99.34	98.98	99.92	86.05	93.14	–	–
MARE		96.55	98.86	99.61	99.98	87.22	93.70	93.75	98.30

on existing Deepfake datasets. The overall loss function is defined as follows:

$$\mathcal{L} = \lambda_1 \mathcal{L}_I + \lambda_2 \mathcal{L}_f + \lambda_3 \mathcal{L}_r \quad (10)$$

where  $\lambda_*$  is the weight parameter to balance each loss component. Secondly, MARE fine-tunes the VLM based on the constructed DMA dataset via a reinforcement learning algorithm. The primary objective is to incentivize the VLM’s reasoning capabilities in Deepfake detection and reasoning. The final reward function  $\mathcal{R}$  is defined as follows:

$$\mathcal{R} = \beta_1 \mathcal{R}_f + \beta_2 \mathcal{R}_a + \beta_3 \mathcal{R}_t + \beta_4 \mathcal{R}_r + \beta_5 \mathcal{R}_{align} \quad (11)$$

where  $\beta_*$  denotes the weight parameter.

**Inference.** Given the face image and question prompts, MARE generates a binary authenticity detection result, followed by an explainable textual description with aligned spatial bounding boxes, as shown in Figure 2.

## 4. Experiment

### 4.1. Experimental setup

**Datasets.** We evaluate MARE on both detection and reasoning generation tasks. The existing Deepfake datasets FaceForensics (FF++) (Rossler et al., 2019), Celeb-DF (Li et al., 2020), WildDeepfake (WDF) (Zi et al., 2020), DFDC (Dolhansky et al., 2020), and DFD (Nicholas Dufour, 2019) are used for detection tasks. The augmented Deepfake multimodal alignment dataset (DMA), based on DDVQA (Zhang et al., 2024), is utilized for the reasoning generation task.

**Evaluation metrics.** In this paper, we utilize Area Under the Curve (AUC) and accuracy (Acc) to measure the binary authenticity detection performance. To evaluate the performance of the reasoning content of VLMs, we measure the identification Acc and F1 by extracting keywords ("fake" or "real") from the generated textual description.

**Implementation details.** The VLM-R1 (Shen et al., 2025) is utilized as the toolkit to fine-tune the VLMs. The reinforcement learning algorithm employs GRPO (Shao et al., 2024). The backbone encoder of FDM is Xception (Chollet, 2017). The fine-tuned VLMs are Qwen2.5-VL-3B (Bai

et al., 2025), Qwen2.5-VL-7B, and InternVL2.5-4B (Chen et al., 2024). The face landmark detection model  $\mathbb{L}(\cdot)$  is MediaPipe Face Mesh.

### 4.2. Detection performance

In this section, we compare the proposed MARE with previous state-of-the-art methods under intra- and fuse-dataset setups, respectively. For intra-dataset comparisons, we cite baseline results from their original papers. For the fuse-dataset experiments, all methods are retrained for fair comparison.

**Intra-dataset performance.** As shown in Table 1, the experimental results show that MARE achieves relatively good performance on both Acc and AUC under intra-dataset comparison. On Celeb-DF, WDF, and DFDC datasets, MARE has achieved performance improvements in both Acc and AUC. It could be observed that MARE achieves state-of-the-art performance on the challenging datasets WDF and DFDC, while it underperforms on the FF++ dataset. This phenomenon could be attributed to the characteristics of FF++, which is generated under five specific Deepfake methods (Deepfakes, Face2Face, FaceShifter, FaceSwap, and NeuralTextures) and constrained scenarios (interviews or news broadcasting). The models may exploit implicit scenario- or identity-specific information to improve the detection performance. In contrast, the FDM of MARE is designed to capture intrinsic forgery traces that are disentangled from image semantics. The experimental results indicate MARE outperforms on both challenging datasets WDF and DFDC. This demonstrates that MARE effectively decouples forgery traces from the high-level semantic information, enabling its superior performance in complex Deepfake detection scenarios.

**Fuse-dataset performance.** To evaluate the proposed MARE’s ability to extract intrinsic forgery traces from different Deepfake scenarios, we introduce the fuse-dataset experiment. In the fuse-dataset experiment, the training subsets of five Deepfake datasets (including FF++, Celeb-DF, WDF, DFDC, and DFD) are merged to create a new training set, and evaluation is conducted on the test subset of each

Table 2. The experimental results of fuse-dataset detection. The best results are presented in red. The second-best values are in blue.

Methods	Venue	FF++		Celeb-DF		WDF		DFDC		DFD	
		Metric: Acc (% ↑) / AUC (% ↑)									
EfficientNet (Tan & Le, 2019)	ICML2019	91.19	94.18	98.65	99.87	80.02	88.22	85.94	93.84	95.63	98.14
ExpD (Ba et al., 2024)	AAAI2024	95.60	98.40	99.42	99.99	80.89	88.02	96.09	99.30	97.53	99.23
SFIC (Guo et al., 2024)	TIFS2024	90.24	90.30	92.86	97.76	76.55	84.37	84.38	91.28	93.74	94.57
M2F2 (Guo et al., 2025)	CVPR2025	97.38	99.25	99.61	99.99	84.86	92.70	95.31	99.16	96.51	98.67
MARE		97.50	99.28	1.00	1.00	87.72	92.66	98.83	99.77	98.25	99.68

Deepfake dataset individually. To ensure a fair comparison, all comparison methods are retrained based on their official open-source implementations. The fuse-dataset experimental results are shown in Table 2. It could be observed that MARE achieves consistent performance improvements on the FF++, Celeb-DF, WDF, DFDC, and DFD datasets. In contrast, comparison method M2F2 shows improved detection performance on Celeb-DF, but exhibits performance degradation on the FF++ and WDF. The primary reason may be the implicit leakage of scenario and identity information, which has impacted its performance in complex Deepfake detection scenarios. The experimental results indicate that MARE could capture the intrinsic forgery traces when faced with diverse Deepfake scenarios. Also, this demonstrates that MARE could decouple intrinsic forgery traces from high-level and diverse semantics.

### 4.3. Reasoning performance

In this section, we conduct both quantitative and qualitative evaluations of the reasoning content generated by MARE. Due to space constraints, some evaluations are presented in appendix A.

**Quantitative result.** To quantitatively evaluate the generated textual description, we extract identification keywords (e.g., "fake" or "real") from the reasoning content. Then, Acc and F1 are calculated based on the ground truth labels. The identification performance of MARE and comparison methods is shown in Table 3.

The pre-trained Qwen (Bai et al., 2025), InternVL (Chen et al., 2024), and LLaVA (Liu et al., 2023) are utilized as baseline models. The results indicate the pre-trained VLMs exhibit suboptimal performance on Deepfake detection and reasoning. The primary reason is that forged face images are often visually difficult to distinguish from genuine ones, since the forgery traces are typically imperceptible. After supervised fine-tuning (SFT) with annotated data, LLaVA achieves significant improvements in both Acc and F1 scores. DDVQA-BLIP (Zhang et al., 2024) and M2F2 combined with SFT to enhance the reasoning capability of VLMs, which achieves further performance improvements. However, the alignment problem in the reasoning process has not been sufficiently explored. MARE constructs a multimodal alignment dataset and designs comprehensive

Table 3. The identification performance of generated textual description on the DMA dataset.

Methods	Fine-tuned	Detection	
		Acc	F1
Qwen	✗	59.41	51.04
InternVL	✗	42.33	47.35
LLaVA	✗	51.41	37.04
LLaVA	✓	86.41	92.10
DDVQA-BLIP	✓	87.49	90.07
M2F2	✓	95.23	96.61
MARE	✓	98.09	97.04

reward functions, and utilizes reinforcement learning to incentivize the VLM to generate accurate and reliable reasoning content. That is the reason that MARE achieves superior performance on both Acc and F1 scores.

**Qualitative performance.** Figure 5 exhibits the reasoning content generated by different models. We employ the API of Qwen-VL and GPT-5 with the prompt "Does this image look fake/real?". Qwen identifies all samples as "real", and generates the textual description that has a generalized and templated style. GPT-5 classifies all samples as "fake". Compared to Qwen, the textual description generated by GPT-5 captures more details, such as eyes, nose, and teeth edges. The results in Figure 5 and Table 3 indicate that the existing general-purpose VLMs have unsatisfactory accuracy in face image authenticity detection. M2F2 achieves improved detection accuracy by introducing expert knowledge. Besides, M2F2 generates fine-grained textual descriptions based on a detailed prompt (e.g., Figure 5 (a) utilizes "The mouth in the image is fake, tell me why..." as the prompt). In contrast, MARE produces reasoning content with text-spatial alignment, which is more aligned with human preferences. It should be noted that MARE uses the prompt "Does this image look fake/real...?", which does not mention specific facial regions. Despite this, MARE could still perceive, locate, and analyze the detected face image, thus generating more accurate and reliable reasoning content.

### 4.4. Ablative Study and Analysis

This section conducts ablation studies to analyze the impact of the VLM backbone within MARE and the specific loss

GT:	Fake	Fake	Fake	Real
Image:				
Qwen:	Real. natural skin texture and noise suggest it's real. <span style="color:red;">✗</span>	Real. Natural skin texture and facial feature show it is real. <span style="color:red;">✗</span>	Real. Natural facial features and lighting suggest authenticity. <span style="color:red;">✗</span>	Real. Natural skin texture and facial features indicate authenticity. <span style="color:green;">✓</span>
GPT-5:	Fake. overly smooth skin, warped mouth eye details suggest manipulation. <span style="color:green;">✓</span>	Fake. facial texture is overly smooth and eye/nose edges look blurred. <span style="color:green;">✓</span>	Fake. smeared facial details and inconsistent lighting around eyes and mouth. <span style="color:green;">✓</span>	Fake. unnaturally smooth skin, overly uniform lighting, and slightly warped teeth/lip edge <span style="color:red;">✗</span>
M2F2:	The mouth is misaligned with other facial parts. <span style="color:green;">✓</span>	The eyes look unnaturally asymmetric. <span style="color:green;">✓</span>	The nose lacks of details, such as pores, fine lines. <span style="color:green;">✓</span>	The person has naturally arched eyebrows. <span style="color:green;">✓</span>
MARE:	The image looks fake because the mouth is unnatural and lacks the fine details typically seen in... {"mouth": [105, 148, 196, 223]} <span style="color:green;">✓</span>	The image looks fake because the eyebrows appear overly symmetrical and lack natural variation... {"eyebrows": [30, 65, 178, 94]} <span style="color:green;">✓</span>	The image looks fake because the nose is unnaturally large and lacks depth, which is inconsistent with... {"nose": [30, 65, 178, 94]} <span style="color:green;">✓</span>	The image looks real because no obvious signs of editing are present. The skin texture and the eyebrows... {"eyebrows": [50, 46, 237, 89], "skin": ...} <span style="color:green;">✓</span>
MARE Bbox:				
	(a)	(b)	(c)	(d)

Figure 5. Examples of reasoning content generated by Qwen, GPT-5, M2F2, and MARE.

components in the FDM. First, we compare the performance of different VLM architectures. Then, based on the best-performing model, we analyze the contribution of  $\mathcal{L}_I$  and  $\mathcal{L}_r$  within the FDM.

**Ablation of VLM architecture.** To evaluate the performance of different VLMs in Deepfake detection and reasoning, we conduct ablation studies on three VLM architectures (InternVL2.5-4B, Qwen2.5-VL-3B, and Qwen2.5-VL-7B) based on DMA dataset. In this ablation study, all experimental settings except the VLM architecture remain fixed, including the FDM and reward functions. The experimental results are shown in Table 4. Qwen2.5-VL models show better performance than the InternVL2.5. This is mainly because Qwen2.5-VL models hold advantages in complex tasks due to their stronger cross-modal understanding abilities. Besides, Qwen2.5-VL-7B has a superior capability than Qwen2.5-VL-3B under the influence of the scaling law.

**Ablation of loss components in FDM.** To verify the effectiveness of the specific loss components within the FDM, we conduct ablation studies on the identity loss  $\mathcal{L}_I$  and reconstruction loss  $\mathcal{L}_r$ . These experiments are performed based on the best-performing Qwen2.5-VL-7B model, and evaluated on the two challenging WDF and DFDC datasets under

Table 4. The identification performance of different VLM architectures base on DMA dataset.

VLM	Detection	
	Acc	F1
InternVL2.5-4B	94.27	90.68
Qwen2.5-VL-3B	95.42	92.68
Qwen2.5-VL-7B	98.09	97.04

Table 5. Ablation study on the specific loss components of the FDM.

$\mathcal{L}_I$	$\mathcal{L}_r$	WDF		DFDC	
		Acc	F1	Acc	F1
		83.62	84.62	94.92	96.07
✓		85.48	86.15	93.75	95.24
✓	✓	87.72	87.82	98.83	99.08

the fuse-dataset setup. The results are shown in Table 5. It could be observed that the performance improves on the WDF dataset after introducing the  $\mathcal{L}_I$ . This indicates that explicit identity supervision helps MARE to decouple identity information from forgery traces features, reducing the interference of identity signals on authenticity detection. Besides, MARE achieves the best performance on both WDF and DFDC after the introduction of  $\mathcal{L}_r$ , which demonstrates that  $\mathcal{L}_r$  imposes a crucial information constraint that ensures the stability of the disentanglement architecture. Therefore, both  $\mathcal{L}_I$  and  $\mathcal{L}_r$  help to improve the ability of MARE in capturing intrinsic forgery traces features.

## 5. Conclusion

In this paper, we propose MARE, a novel framework designed to enhance the accuracy and reliability of VLMs in Deepfake detection and reasoning. MARE aims to generate text-spatially aligned reasoning content within the RLHF paradigm. We first construct a human feedback annotation dataset and design the reward mechanism. A Deepfake multimodal alignment dataset is introduced to augment the existing image-text Deepfake dataset with aligned spatial localization information. To effectively incentivize the reasoning capability of VLM, MARE designs a comprehensive reward mechanism comprising five functions: format, accuracy, text relevance, ROI, and alignment rewards. Besides, a forgery disentanglement module is introduced to capture intrinsic forgery traces for precise authenticity identification, which disentangles the face image into identity, structural, and forgery traces features. Extensive quantitative and qualitative experiments validate that MARE achieves state-of-the-art performance in Deepfake detection and reasoning. We observe that existing evaluation methodologies, such as accuracy, AUC, and standard NLP metrics, are becoming insufficient for assessing the logical consistency and explain-

ability of explainable Deepfake detection. In the future, we will explore more effective evaluation methodologies for generative Deepfake reasoning content.

## Impact Statement

This paper presents work whose goal is to advance the field of Machine Learning, specifically in the domain of AI safety and multimedia forensics. The proposed MARE aims to mitigate the spread of malicious misinformation and protect the security of the face image by providing explainable Deepfake detection. Our work enables human to better understand why an image is classified as forged by providing text-spatially aligned reasoning content. All experiments in this study are conducted on publicly available datasets.

## References

Ba, Z., Liu, Q., Liu, Z., Wu, S., Lin, F., Lu, L., and Ren, K. Exposing the deception: Uncovering more forgery clues for Deepfake detection. In *Proceedings of the AAAI Conference on Artificial Intelligence*, pp. 719–728, 2024.

Bai, S., Chen, K., Liu, X., Wang, J., Ge, W., Song, S., Dang, K., Wang, P., Wang, S., Tang, J., et al. Qwen2.5-VL technical report. *arXiv preprint arXiv:2502.13923*, 2025.

Cao, J., Ma, C., Yao, T., Chen, S., Ding, S., and Yang, X. End-to-end reconstruction-classification learning for face forgery detection. In *Proceedings of the IEEE/CVF Conference on Computer Vision and Pattern Recognition*, pp. 4113–4122, June 2022.

Chen, Z., Wang, W., Cao, Y., Liu, Y., Gao, Z., Cui, E., Zhu, J., Ye, S., Tian, H., Liu, Z., et al. Expanding performance boundaries of open-source multimodal models with model, data, and test-time scaling. *arXiv preprint arXiv:2412.05271*, 2024.

Chiang, W.-L., Li, Z., Lin, Z., Sheng, Y., Wu, Z., Zhang, H., Zheng, L., Zhuang, S., Zhuang, Y., Gonzalez, J. E., and et al. Vicuna: An open-source chatbot impressing gpt-4 with 90% chatgpt quality. pp. 6, 2023. URL <https://vicuna.lmsys.org>.

Chollet, F. Xception: Deep learning with depthwise separable convolutions. In *Proceedings of the IEEE conference on computer vision and pattern recognition*, pp. 1251–1258, 2017.

Dolhansky, B., Bitton, J., Pflaum, B., Lu, J., Howes, R., Wang, M., and Ferrer, C. C. The Deepfake detection challenge (DFDC) dataset. *arXiv preprint arXiv:2006.07397*, 2020.

Guo, X., Song, X., Zhang, Y., Liu, X., and Liu, X. Rethinking vision-language model in face forensics: Multi-modal interpretable forged face detector. In *Proceedings of the Computer Vision and Pattern Recognition Conference*, pp. 105–116, 2025.

Guo, Z., Jia, Z., Wang, L., Wang, D., Yang, G., and Kasabov, N. Constructing new backbone networks via space-frequency interactive convolution for Deepfake detection. *IEEE Transactions on Information Forensics and Security*, 19:401–413, 2024.

Huang, Z., Hu, J., Li, X., He, Y., Zhao, X., Peng, B., Wu, B., Huang, X., and Cheng, G. SIDA: Social media image Deepfake detection, localization and explanation with large multimodal model. In *Proceedings of the Computer Vision and Pattern Recognition Conference*, pp. 28831–28841, 2025.

Jose, L. P., Smith, E., Gregory, D., and Bevin, B. More articles are now created by ai than humans. 2025. URL <https://graphite.io/five-percent>.

Li, J., Li, H., Erfani, S. M., Feng, L., Bailey, J., and Liu, F. Visual-text cross alignment: Refining the similarity score in vision-language models. In *Proceedings of the 41st International Conference on Machine Learning*, volume 235, pp. 28018–28039. PMLR, 2024.

Li, T., Huang, Z., Wen, H., He, Y., Lyu, S., Wu, B., and Cheng, G. RAIDX: A retrieval-augmented generation and GRPO reinforcement learning framework for explainable Deepfake detection. In *Proceedings of the 33rd ACM International Conference on Multimedia*, pp. 11746–11755, 2025a.

Li, Y., Yang, X., Sun, P., Qi, H., and Lyu, S. Celeb-DF: A large-scale challenging dataset for Deepfake forensics. In *Proceedings of the IEEE/CVF Conference on Computer Vision and Pattern Recognition*, June 2020.

Li, Z., Wu, X., Du, H., Liu, F., Nghiêm, H., and Shi, G. A survey of state of the art large vision language models: Alignment, benchmark, evaluations and challenges. *arXiv preprint arXiv:2501.02189*, 2025b.

Liu, H., Li, C., Wu, Q., and Lee, Y. J. Visual instruction tuning. In *Advances in Neural Information Processing Systems*, volume 36, pp. 34892–34916. Curran Associates, Inc., 2023.

Meng, F., Du, L., Liu, Z., Zhou, Z., Lu, Q., Fu, D., Han, T., Shi, B., Wang, W., He, J., et al. MM-Eureka: Exploring the frontiers of multimodal reasoning with rule-based reinforcement learning. *arXiv preprint arXiv:2503.07365*, 2025.

Nicholas Dufour, Andrew Gully, P. K. Deepfakes detection dataset. 2019. URL <https://www.kaggle.com/datasets/sanikatiwarekar>.

Rossler, A., Cozzolino, D., Verdoliva, L., Riess, C., Thies, J., and Niessner, M. Faceforensics++: Learning to detect manipulated facial images. In *Proceedings of the IEEE/CVF International Conference on Computer Vision*, 2019.

Shao, Z., Wang, P., Zhu, Q., Xu, R., Song, J., Bi, X., Zhang, H., Zhang, M., Li, Y., Wu, Y., et al. DeepSeekMath: Pushing the limits of mathematical reasoning in open language models. *arXiv preprint arXiv:2402.03300*, 2024.

She, H., Hu, Y., Liu, B., Li, J., and Li, C.-T. Using graph neural networks to improve generalization capability of the models for Deepfake detection. *IEEE Transactions on Information Forensics and Security*, 19:8414–8427, 2024.

Shen, H., Liu, P., Li, J., Fang, C., Ma, Y., Liao, J., Shen, Q., Zhang, Z., Zhao, K., Zhang, Q., et al. VLM-R1: A stable and generalizable r1-style large vision-language model. *arXiv preprint arXiv:2504.07615*, 2025.

Shiohara, K. and Yamasaki, T. Detecting Deepfakes with self-blended images. In *Proceedings of the IEEE/CVF conference on computer vision and pattern recognition*, pp. 18720–18729, 2022.

Tan, M. and Le, Q. Efficientnet: Rethinking model scaling for convolutional neural networks. In *International conference on machine learning*, pp. 6105–6114. PMLR, 2019.

Wang, W., Wei, F., Dong, L., Bao, H., Yang, N., and Zhou, M. MiniLM: Deep self-attention distillation for task-agnostic compression of pre-trained transformers. In *Advances in Neural Information Processing Systems*, volume 33, pp. 5776–5788, 2020.

Xie, C., Wang, B., Kong, F., Li, J., Liang, D., Zhang, G., Leng, D., and Yin, Y. FG-CLIP: Fine-grained visual and textual alignment. In *Proceedings of the 42nd International Conference on Machine Learning*. PMLR, 2025.

Xu, W., Lu, W., and Luo, X. Weakly supervised multimodal temporal forgery localization via multitask learning. *arXiv preprint arXiv:2508.02179*, 2025a.

Xu, W., Wu, J., Lu, W., Luo, X., and Wang, Q. A multimodal deviation perceiving framework for weakly-supervised temporal forgery localization. In *Proceedings of the 33rd ACM International Conference on Multimedia*, pp. 11581–11589, 2025b.

Xu, Y., Liang, J., Jia, G., Yang, Z., Zhang, Y., and He, R. TALL: Thumbnail layout for Deepfake video detection. In *Proceedings of the IEEE/CVF International Conference on Computer Vision*, pp. 22658–22668, 2023.

Yin, Q., Lu, W., Cao, X., Luo, X., Zhou, Y., and Huang, J. Fine-grained multimodal Deepfake classification via heterogeneous graphs. *International Journal of Computer Vision*, 132(11):5255–5269, 2024.

Yu, P., Fei, J., Gao, H., Feng, X., Xia, Z., and Chang, C. H. Unlocking the capabilities of vision-language models for generalizable and explainable Deepfake detection. In *Proceedings of the 42nd International Conference on Machine Learning*. PMLR, 2025.

Zhai, S., Bai, H., Lin, Z., Pan, J., Tong, P., Zhou, Y., Suhr, A., Xie, S., LeCun, Y., Ma, Y., et al. Fine-tuning large vision-language models as decision-making agents via reinforcement learning. *Advances in neural information processing systems*, 37:110935–110971, 2024.

Zhang, B., Yin, Q., Lu, W., and Luo, X. Deepfake detection and localization using multi-view inconsistency measurement. *IEEE Transactions on Dependable and Secure Computing*, 22(2):1796–1809, 2025a.

Zhang, Y., Colman, B., Guo, X., Shahriyari, A., and Bharaj, G. Common sense reasoning for Deepfake detection. In *European conference on computer vision*, pp. 399–415. Springer, 2024.

Zhang, Y.-F., Yu, T., Tian, H., Fu, C., Li, P., Zeng, J., Xie, W., Shi, Y., Zhang, H., Wu, J., et al. MM-RLHF: The next step forward in multimodal LLM alignment. *arXiv preprint arXiv:2502.10391*, 2025b.

Zhao, H., Zhou, W., Chen, D., Wei, T., Zhang, W., and Yu, N. Multi-attentional Deepfake detection. In *Proceedings of the IEEE/CVF Conference on Computer Vision and Pattern Recognition*, pp. 2185–2194, June 2021.

Zi, B., Chang, M., Chen, J., Ma, X., and Jiang, Y.-G. Wild-Deepfake: A challenging real-world dataset for Deepfake detection. In *Proceedings of the 28th ACM International Conference on Multimedia*, pp. 2382–2390, 2020.

## A. More experimental analysis

Q&A	Image	Qwen/Loc	Qwen/Reasoning	MARE/Loc	MARE/Reasoning
Q: Does the person's nose look real/fake? A: The person's nose looks very <b>fake</b> because the nose lacks of subtle details, such as pores, fine lines.			"The person's nose looks <b>real</b> because there are no visible signs of artificial enhancement or distortion." <span style="color:red;">X</span>		"The person's nose looks <b>fake</b> because it lacks the natural texture and shading found in real photographs. This is evident in the smoothness and uniformity of the skin around the nose area." <span style="color:green;">✓</span>
Q: Does the person's mouth look real/fake? A: The person's mouth looks <b>fake</b> . The person's mouth looks very fake because the mouth looks too rigid to convey expressions.			"The person's mouth looks <b>real</b> because it has natural curvature and shading." <span style="color:red;">X</span>		"The person's mouth looks <b>fake</b> because the texture and detail around the mouth area appear unnatural, which is often a sign of digital manipulation. The lips do not have the natural curvature and shading expected in a real mouth." <span style="color:green;">✓</span>
Q: Does the person's mouth look real/fake? A: The person's mouth looks a bit <b>fake</b> because the teeth look unnatural coloring.			"The person's mouth looks <b>real</b> because it has a natural shape and coloration with realistic texture and shading." <span style="color:red;">X</span>		"The person's mouth looks <b>fake</b> because it lacks the natural texture and detail of a real human mouth. The lips appear unnaturally smooth and uniform." <span style="color:green;">✓</span>
Q: Do the person's eyebrows look real/fake? A: The person's eyebrows look very <b>fake</b> because the eyebrows look asymmetric.			"The person's eyebrows look <b>real</b> because they appear symmetrical and uniform, which could suggest enhancement." <span style="color:red;">X</span>		"The person's eyebrows look <b>fake</b> because they appear overly symmetrical and smooth, lacking natural imperfections. This is evident in the entire eyebrow area." <span style="color:green;">✓</span>
Q: Does the image looks real/fake? A: The image looks <b>real</b> . The person has smooth skin, arched eyebrows, round eyes, straight nose, thin mouth.			"The image looks <b>real</b> because it shows natural skin texture, lighting, and facial features without any signs of manipulation." <span style="color:green;">✓</span>		"The image looks <b>real</b> because the facial features and skin texture appear natural and consistent with human characteristics." <span style="color:green;">✓</span>

Figure 6. Examples of reasoning content generated by pre-trained Qwen2.5-VL-7B (Qwen) and MARE. Column *Q&A* indicates human annotated question prompt and answer. Column *Image* is the detected face image. Column *Qwen/Loc* and *MARE/Loc* indicate the spatial bounding boxes generated by Qwen and MARE, respectively. Column *Qwen/Reasoning* and *MARE/Reasoning* indicate the textual reasoning content generated by Qwen and MARE, respectively.

### A.1. Deepfake detection and reasoning

Figure 6 represents representative Deepfake detection and reasoning samples from MARE and pre-trained VLM. To be more concise, the spatial bounding boxes predicted by the model have been drawn directly onto the face image.

As observed in Section 4.3, the existing pre-trained Qwen model tends to misclassify forged face images as "real", with obvious deviations in spatial bounding boxes (as shown in the third column). Qwen also shows an unsatisfactory alignment between the generated textual reasoning and spatial bounding boxes. For example, for the sample in the first row, the textual reasoning content of Qwen focuses on forgery traces in the nose, but the bounding boxes contain both the eyes and the nose. For the samples in the second row, the text describes the mouth, but the spatial bounding boxes locate the facial and skin texture.

In contrast, MARE exhibits better accuracy and reliability in Deepfake detection and reasoning. MARE achieves precise authenticity identification by introducing the forgery disentanglement module to capture intrinsic forgery traces. Based on the constructed Deepfake multimodal alignment (DMA) dataset, MARE incentivizes the VLM to generate more accurate and reliable reasoning content under the RLHF paradigm. As shown in the fifth column of Figure 6, MARE achieves significant improvements in spatial localization ac-

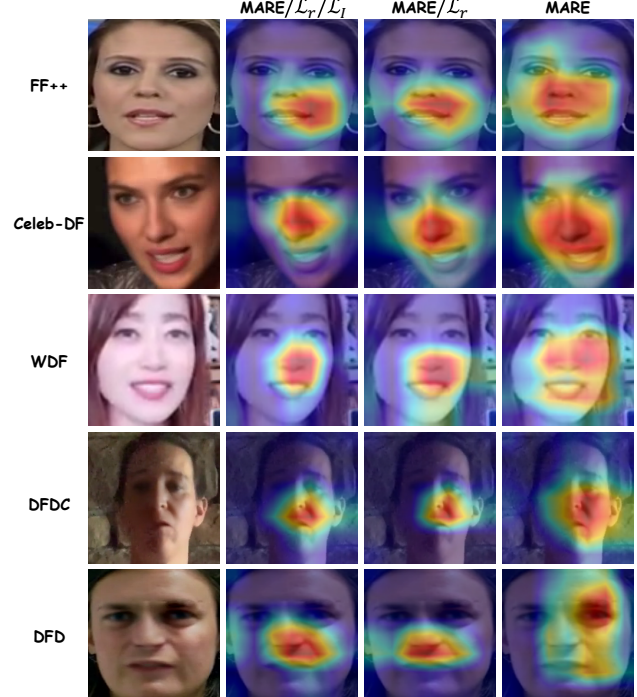


Figure 7. Examples of forged attention maps from FF++, Celeb-DF, WDF, DFDC, and DFD dataset. Column *MARE/L<sub>r</sub>/L<sub>I</sub>* indicates the attention maps of MARE removing loss  $L_r$ . Column *MARE/L<sub>r</sub>/L<sub>I</sub>* indicates the attention maps of MARE removing loss  $L_r$  and  $L_I$ .

curacy. Furthermore, the generated textual reasoning maintains high alignment with the spatial bounding boxes, which is better aligned with human preferences.

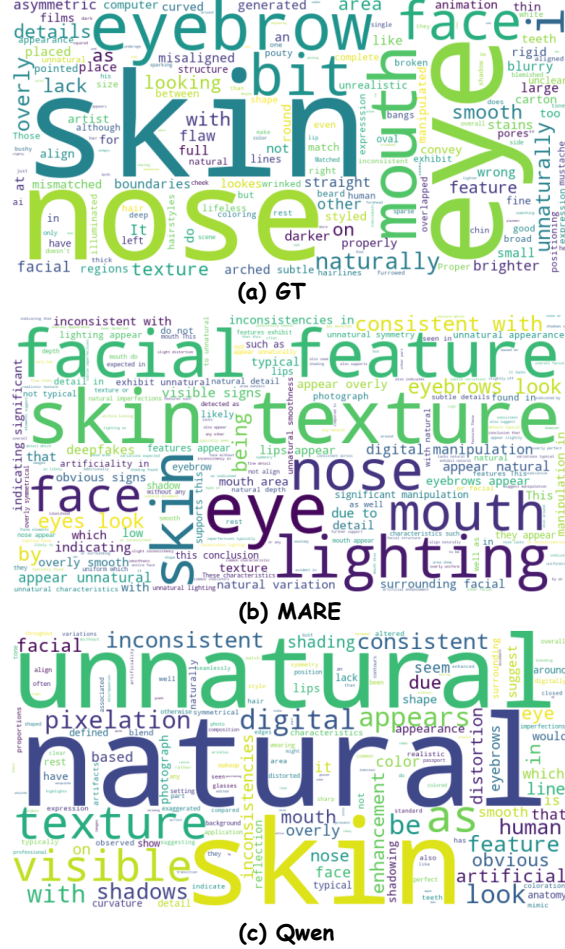


Figure 8. Visualization of word clouds derived from human annotated text (GT), MARE’s reasoning content, and Qwen’s reasoning content.

## A.2. Visualization of forged attention maps

To more vividly display MARE’s attention maps when capturing forgery traces, we visualize some examples in this section. As shown in Figure 7, it could be observed that MARE focuses not only on specific facial regions but also on facial boundaries. During the Deepfake synthesis process, the blending of source and target faces typically leaves intrinsic forgery traces at the facial boundaries. The attention maps in Figure 7 indicate that MARE attempts to capture intrinsic forgery traces from multiple perspectives to enhance the accuracy of Deepfake authenticity identification.

## A.3. Visualization of word clouds

To provide more intuitive analysis of explainable textual description, Figure 8 visualizes the word clouds generated from human annotated text, MARE’s reasoning content, and Qwen’s reasoning content. It could be observed that both human annotated text and MARE’s reasoning focus on analyzing specific facial regions. For example, “nose”, “eyes”, and “mouth” are the high-frequency words in the word clouds of GT and MARE. In contrast, the Qwen exhibits limited attention to the facial regions during the reasoning process. Figure 8 indicates the reasoning content generated by MARE for Deepfake detection and reasoning aligns more closely with human preferences.

## B. Facial region set

Table 6 shows the predefined facial region set  $\mathcal{P}_{key}$ . We categorize the face into 12 distinct regions (e.g., skin, nose, left/right eye). For each region, a set of associated keywords is defined, which cover synonyms and related terms commonly found in textual descriptions. This mapping serves as the basis for the Deepfake multimodal alignment dataset construction.

Specifically, it is utilized to retrieve and extract specific regions mentioned in the textual description. Then, the spatial information could be obtained by a face landmark detection model.

Facial region	Associated keywords
skin	skin, cheek, forehead, complexion, dermal, face
nose	nose, nostril, nasal
mouth	mouth, lip, lips
teeth	tooth, teeth
left_eye	left eye, left-eye, 1 eye, lefteye, eye, ocular
right_eye	right eye, right-eye, r eye, righteye, eye, ocular
left_eyebrow	left eyebrow, left brow, left-eyebrow, eyebrow, brow
right_eyebrow	right eyebrow, right brow, right-eyebrow, eyebrow, brow
chin	chin, jaw, jawline, lower face
beard	beard, mustache, moustache, goatee
hairline	hairline, hair line, hair
ear	ear, ears

Table 6. The predefined keyword set about facial regions and corresponding textual keywords.